Mutual Inductance Estimation Based Sensorless Adaptive Variance Controller for Doubly Fed Induction Generator

Anuprabha Ravindran Nair, *Graduate Student Member, IEEE*, Rojan Bhattarai, *Member, IEEE*, and Sukumar Kamalasadan, *Senior Member, IEEE*

***Abstract*—This article presents a novel robust adaptive speed control architecture that allows doubly fed induction generator (DFIG) to operate independently of any speed sensors or position encoders. The proposed speed sensorless control based on modified minimum variance adaptive control based speed observer makes the system robust to machine parameter variations and sensor malfunctions. The observer is formulated using a rotor current based reference adaptive system. To ensure robustness to current sensor failure, a modified adaptive rotor side converter control loop is proposed. The online identification for the adaptive control logic is based on the recursive least square estimation technique while the adaptive control law is based on an extended version of the minimum variance control algorithm. To ensure improved dynamic performance for the proposed control, a modification for the terminal voltage control loop is proposed. The reactive power reference for the vector control loop is calculated considering the rotor current component responsible for reactive power generation. The performance of the proposed control architecture is validated on a 1.5 MW DFIG modeled in MATLAB/Simulink and experimentally verified on hardware.**

***Index Terms*—Adaptive control, doubly fed induction generator (DFIG), extended minimum variance controller (EMVC), minimum recursive least squares (RLS), sensorless control.**

I. Introduction

DOUBLY fed induction generator (DFIG) based wind energy conversion systems are most prominent due to its ability to work with a low-rated converter. The traditional reference frame-based vector control approach is widely used for decoupled control of real power (P) and reactive power (Q) output of DFIG. The vector control approach relies on measurement data such as rotor and stator currents and speed. This highlights the dependency of the conventional approach to devices like sensors that are prone to failure. Some of the earlier works in speed sensorless operation of DFIG uses an open-loop method for estimating the rotor current to analyze the rotor position [1], [2]. Other approaches based on the phase-locked loop and hysteresis controller are also discussed in the literature. But most of these designs are based on static controllers which are not robust to machine parameter variations. On the closed-loop form, small-signal analysis of model reference adaptive system (MRAS)-based sensorless control of DFIG is discussed in [3]. Furthermore, in [4] a modified MRAS-based speed observer is proposed where slip frequency is estimated using the reactive power-based model considering the estimation of machine mutual inductance. Parameter estimation based speed sensorless control of DFIG using slide mode control is discussed in [5]. The estimation techniques derive the rotor position and speed during start-up and grid synchronization. A sensorless stator flux orientated control of DFIG in which the slip angle is estimated from air gap power is proposed in [6]. Several variations of sensorless control of DFIG are discussed in [7]–[10] and parameter estimation methods are discussed in [11] and [12]. In [13], the need for parameter estimation technique in a sensorless approach is discussed. Similar techniques are also proposed in [14]–[16] and [17]–[19].

Most of the work discussed in the literature rely on static controllers, which shows deteriorated performance during dynamic operatic conditions. To this effect, online identification based speed sensorless adaptive control logic is discussed in [20]–[24]. A detailed analysis of some of the existing sensorless control techniques of DFIG is presented in [25]–[28] but these approaches are not comprehensive. For example, a sensorless DFIG control method based on a modified hill climb search method is discussed in [25]. Even though the adverse effect of L_m on reference direct component of the current is discussed, this work does not discuss the robustness of the proposed control during machine parameter variations. In [26], rotor current sensorless operation is discussed but as the rotor current sensor fails the operation is affected adversely.

Considering these facts, a parametrically robust sensorless control of DFIG based on adaptive control was proposed in our earlier work [29]. The work introduces a recursive least square (RLS) identification based extended minimum variance control (EMVC) architecture. The modified minimum variance architecture makes the sensorless system robust to parameter

Manuscript received April 15, 2020; revised July 23, 2020; accepted August 25, 2020. Date of publication September 16, 2020; date of current version November 19, 2020. Paper 2020-IACC-0083.R1, presented at the 2019 IEEE Energy Conversion Congress and Exposition, Baltimore, MD, USA, 29 Sep. to Oct. 3 and approved for publication in the IEEE TRANSACTIONS ON INDUSTRY APPLICATION by the Energy Systems Committee of the IEEE industry Applications Society. This work was supported by the National Science Foundation under Grant ECCS-1810174 awarded to the third author. *(Corresponding author: Sukumar Kamalasadan.)*

The authors are with the Department of Electrical and Computer Engineering, University of North Carolina at Charlotte, Charlotte, NC 28223 USA (e-mail: anair8@uncc.edu; rbhattar@uncc.edu; skamalas@uncc.edu).

Color versions of one or more of the figures in this article are available online at https://ieeexplore.ieee.org.

Digital Object Identifier 10.1109/TIA.2020.3024351

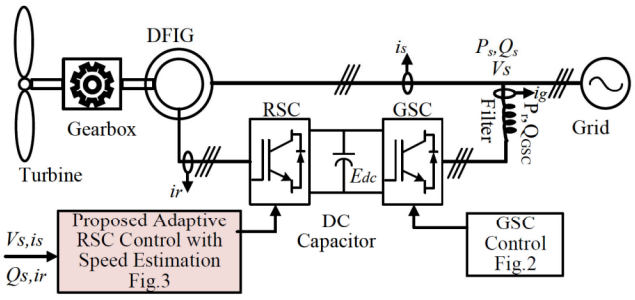

Fig. 1. DFIG-based WECS.

variations. However, the speed observer proposed in earlier work relies on the measured rotor current to tune the adaptive model of MRAS based observer. In this article, an extended rotor side converter (RSC) adaptive control logic based speed sensorless control of DFIG is proposed. Compared to the conventional control approach, the architecture proposed here is independent of any speed sensors and the effect of machine parameter variations. The most prevalent features of the proposed technique include.

1) The ability to perform independently in the advent of speed and current sensor malfunctions.
2) Ability to auto-tune and enhanced stability and reliability over a wider operating range.
3) Robustness to the variations in physical parameters due to temperature or other physical conditions.

The major contributions of the proposed work are as follows.

1) Modified adaptive RSC control loop that ensures reliable operation of proposed sensorless control during rotor current sensor failures.
2) Accurate estimation of the dynamic transfer function, which helps operate in wide dynamic conditions.
3) EMVC algorithm that makes the architecture robust to dynamic electrical variations.
4) Improved dynamic performance capability during parameter variations due to the modified terminal voltage loop.
5) Scalable and feasible for real-life implementations.

The rest of this article is organized as follows: Section II discusses the mathematical model of the reference frame theory-based conventional control architecture of DFIG. Section III discusses the mathematical framework for the proposed control including speed observer, EMVC algorithm framework for adaptive sensorless control, adaptive RSC control, and the modified outer terminal voltage loop of the proposed system. Section IV discusses the experimental results including the scalability results on the real-life grid model and Section V discusses the conclusion.

II. Modeling and Control of Dfig

Grid-connected DFIG based wind energy conversion system (WECS) is shown in Fig. 1. As the name suggests, the DFIG-based system is doubly fed with stator directly connected to grid and rotor interconnected to the grid via back to back converters. These power electronic-based converters are then controlled using proper control logic implemented based on a dq reference frame named as vector control. This approach enables the independent control of the real and reactive power output. There is a common dc-link between the RSC and grid side converters (GSC) and RSC regulates the power output to the grid.

A. Mathematical Model of DFIG

With $V_{ds/r}$, $I_{ds/r}$, and $V_{qs/r}$, $I_{qs/r}$ as the stator side and rotor side voltage and current in dq frame, the voltage equations governing the stator side and rotor side can be represented as given below

$$Vds = RsIds + p\lambda ds - \omega\lambda qs \tag{1}$$

$$Vqs = RsIqs + p\lambda qs + \omega\lambda ds \tag{2}$$

$$Vdr = RrIdr + p\lambda dr - (\omega - \omega r)\lambda qr \tag{3}$$

$$Vqr = RrIqr + p\lambda qr + (\omega - \omega r)\lambda dr \tag{4}$$

where $\lambda_{d/q,s/r}$ corresponds to the d and q axis stator and rotor flux, respectively. ω represents the synchronous speed of the grid frequency, ω_r corresponds to rotor speed at slip frequency, and the stator and rotor voltages are dependent on flux dynamics.

The dynamic equations governing the stator and rotor flux linkage in $d-q$ frame are given by

$$\lambda ds = LsIds + LmIdr \tag{5}$$

$$\lambda qs = LsIqs + LmIqr \tag{6}$$

$$\lambda dr = LrIdr + LmIds \tag{7}$$

$$\lambda qr = LrIqr + LmIqs. \tag{8}$$

Electromagnetic torque in $d-q$ frame can be represented in terms of currents and flux as follows:

$$Te = \frac{3P}{2}(Iqs\lambda ds - Ids\lambda qs). \tag{9}$$

The output of the RSC is assumed to be oriented along the stator flux vector. The phase of the stator flux called slip angle is calculated from the two phase stator flux components formulated as follows:

$$\lambda_{\alpha\text{stator}} = \int (V_{\alpha\ \text{stator}} + R_s I_{\alpha\text{stator}})dt \tag{10}$$

$$\lambda_{\beta\text{stator}} = \int (V_{\beta\text{stator}} + R_s I_{\beta\text{stator}})dt. \tag{11}$$

In this work, the $d-q$ reference frame is assumed to be oriented along the stator flux. Hence, according to the assumed convention, q axis stator flux and d axis stator voltage will be zero. Hence, the stator real power output, P can be controlled by i_{qr} and reactive power output, Q by i_{dr}. The stator flux angle is calculated from (10) and (11) as follows:

$$\theta e = \tan^{-1}\frac{\lambda_{\beta\text{stator}}}{\lambda_{\alpha\text{stator}}}. \tag{12}$$

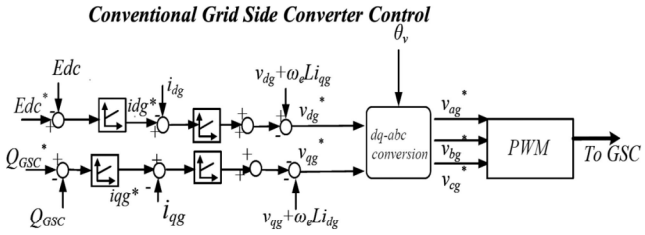

Fig. 2. Conventional GSC Control.

B. Conventional GSC Control Architecture

In the conventional GSC control architecture (Fig. 2), the voltage equations across the grid side filter is

$$\begin{bmatrix} V_{a\text{inv}} \\ V_{b\text{inv}} \\ V_{c\text{inv}} \end{bmatrix} = \mathrm{R} \begin{bmatrix} I_{a\text{inv}} \\ I_{b\text{inv}} \\ I_{\text{inv}} \end{bmatrix} + \mathrm{pL} \begin{bmatrix} I_{a\text{inv}} \\ I_{b\text{inv}} \\ I_{c\text{inv}} \end{bmatrix} + \begin{bmatrix} V_{ag} \\ V_{bg} \\ V_{cg} \end{bmatrix} \tag{13}$$

where R and L are the line parameters, $V_{abc\text{inv}}$ is the inverter output voltage, $I_{abc\text{inv}}$ is the inverter output current, V_{abcg} is the grid voltage. The abovementioned equation in a synchronously dq reference frame rotating at ω_{e} rad/s can be represented as follows:

$$\begin{aligned} \mathrm{v_{dgi}} &= \mathrm{Ri_{dg}} + \mathrm{pLi_{dg}} - \omega_{\mathrm{e}}\mathrm{Li_{qg}} + \mathrm{v_{dg}} \\ \mathrm{v_{qgi}} &= \mathrm{Ri_{qg}} + \mathrm{pLi_{qg}} - \omega_{\mathrm{e}}\mathrm{Li_{dg}} + \mathrm{v_{qg}} \end{aligned} \tag{14}$$

where ω_{e} is the angular frequency of the supply voltage, $\mathrm{i_{dg}}$ and $\mathrm{i_{qg}}$ is the d-axis and q-axis current from inverter, respectively, $\mathrm{v_{dg}}$ and $\mathrm{v_{qg}}$ is the d-axis and q-axis grid voltage, respectively, and $\mathrm{v_{dgi}}$ and $\mathrm{v_{qgi}}$ is the d-axis and q-axis output voltage of the inverter.

III. Proposed Adaptive RSC Control With Speed Estimation Framework

The adaptive control framework discussed here is an extended version of minimum variance control (MVC), viz., EMVC. The architecture is illustrated in Fig. 3. It consists of a proposed speed estimation, outer voltage control loop, and adaptive RSC control framework.

A. Proposed Speed Estimation Framework

1) Speed Observer: The speed observer is based on an MRAS technique which estimates the rotor current. The estimated value of the rotor current is then compared to the actual current that is measured and the error is reduced based on an online algorithm. The measured rotor current I_r can be derived as follows:

$$I_r = \frac{(\varphi_s + L_s I_s)}{L_m} \exp^{-j\theta r} \tag{15}$$

where θ_r is the rotor position measured with respect to the stationary reference frame.

Correspondingly the estimated rotor current based on the estimated angle θ_{rest} can be represented as follows:

$$I_{\text{rest}} = \frac{(\varphi_s + L_s I_s)}{L_m} \exp^{-j\theta \text{rest}} \tag{16}$$

The currents (estimated and actual) match when the angular positions are within the threshold represented by an error function ϵ. This can be expressed as the angle between dot and cross products of the estimated and actual rotor angles [29].

$$\epsilon = \frac{I_r \times I_{\text{rest}} \sin\theta_{\text{err}}}{I_r \bullet I_{\text{rest}} \cos\theta_{\text{err}}} \tag{17}$$

where θ_{err} is the angle difference between actual and estimated rotor current.

2) Identification Methodology: The proposed adaptive control approach utilizes an online RLS technique for identification. The details are discussed in [29] and [30]. The discrete Z domain representation of the identifier can be defined as follows:

$$\frac{\epsilon_m(k)}{\omega_{\text{rest}}(k)} = \frac{b_1 z^{-1} + b_2 z^{-2}}{1 + a_1 z^{-1} + a_2 z^{-2}}. \tag{18}$$

RLS identifies the coefficients a_1, a_2, b_1, and b_2 at every instant. The dynamic system transfer function as defined by (18) will identified at every instant. The output of the transfer function model error at any instant k is defined as follows:

$$\begin{aligned} \epsilon_m(k) = & -a_1\epsilon(k-1) - a_2\epsilon(k-2) \\ & + b_1\omega_{\text{rest}}(k-1) + b_2\omega_{\text{rest}}(k-2). \end{aligned} \tag{19}$$

3) EMVC Framework: Considering a second-order transfer function for the speed observer in (18), a control auto regressive moving average model representation for the error can be represented as follows:

$$\epsilon(k) = \frac{B(q^{-1})}{A(q^{-1})} \times \omega_{\text{rest}}(k) + \frac{C(q^{-1})}{A(q^{-1})} \times E(k) \tag{20}$$

where $\epsilon(k)$ represents the model output which is the error in rotor angle, $\omega_{\text{rest}}(k)$ represents the estimated speed which is the input to the model and model error or noise is represented in the form of $E(k)$.

From (20) the model error $E(k)$ with d as the time delay of the process can be represented as follows:

$$E(k) = \frac{A(q^{-1})\epsilon(k) - B(q^{-1})(q^{-d})\omega_{\text{rest}}(k)}{C(q^{-1})}. \tag{21}$$

If

$$\frac{C(q^{-1})}{A(q^{-1})} = F(q^{-1}) + \frac{G(q^{-1})}{A(q^{-1})} \tag{22}$$

then

$$\epsilon(k) = \frac{B(q^{-1})}{A(q^{-1})}\omega_{\text{rest}}(k) + F(q^{-1})E(k) + \frac{G(q^{-1})}{A(q^{-1})}E(k). \tag{23}$$

From (23), using algebraic identities

$$\begin{aligned} \epsilon(k) = & F(q^{-1})E(k) + \frac{G(q^{-1})}{C(q^{-1})}\epsilon(k) \\ & + \frac{B(q^{-1})}{C(q^{-1})}F(q^{-1})\omega_{\text{rest}}(k). \end{aligned} \tag{24}$$

The proposed control algorithm defines the controlled output ω_{rest}. The variance of the abovementioned equation is minimum

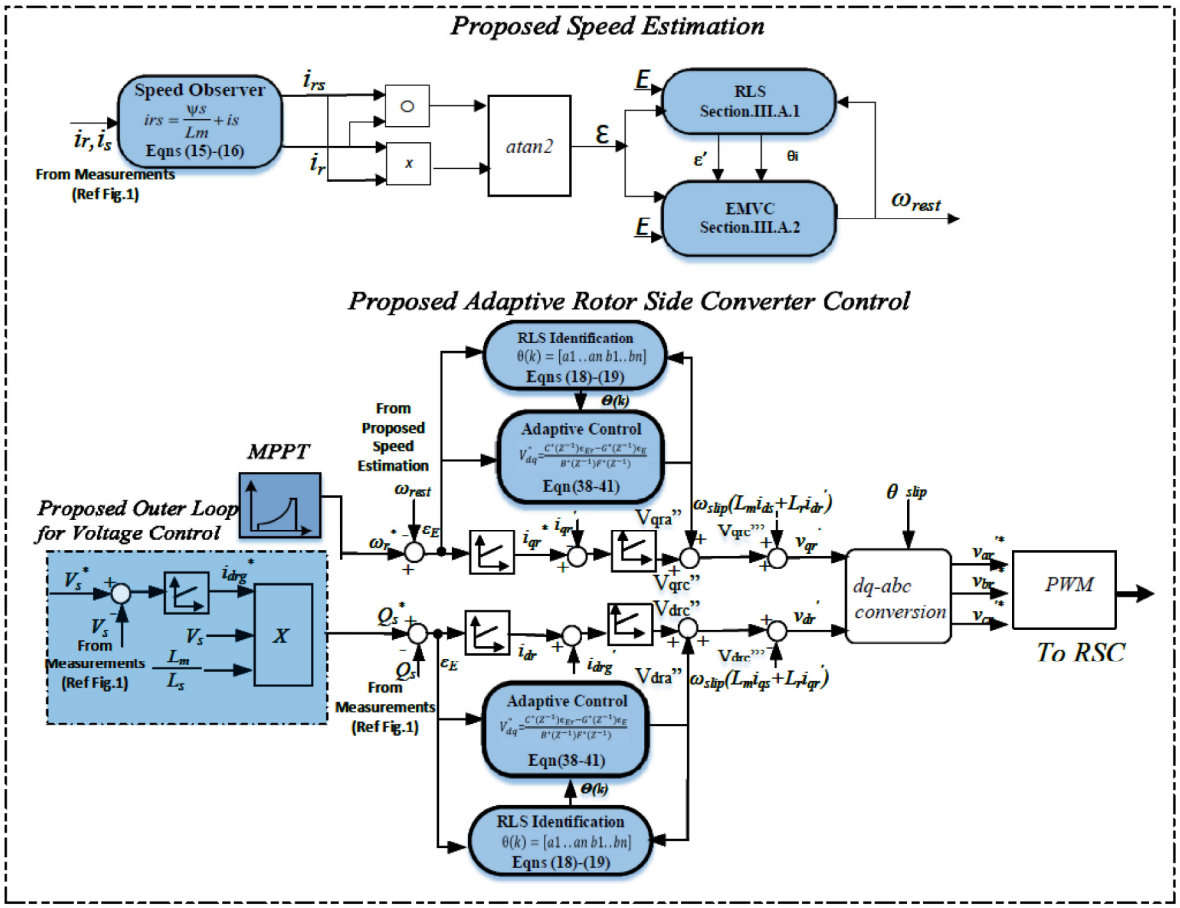

Fig. 3. Proposed adaptive RSC control with speed estimation.

when

$$\frac{G(q^{-1})}{C(q^{-1})}\epsilon(k)+\frac{B(q^{-1})}{C(q^{-1})}F(q^{-1})\omega_{\text{rest}}(k)=0 \tag{25}$$

where

$$\omega_{\text{rest}}(k)=-\frac{G(q^{-1})}{B(q^{-1})F(q^{-1})}\epsilon(k). \tag{26}$$

With this the controller output becomes

$$\epsilon(k)=F(q^{-1})E(k) \tag{27}$$

with the polynomials defined as follows:

$$F(q^{-1})=1 \tag{28}$$

$$G(q^{-1})=(c1-a1)(q^{-1})+(c2-a2)(q^{-2}). \tag{29}$$

The controlled input to the plant, ω_{rest} is estimated based on the current value and past values of the output and error signals as given by

$$\omega_{\text{rest}}(k)=-\frac{(c1-a1)(q^{-1})+(c2-a2)(q^{-2})}{b1(q^{-1})+b2(q^{-2})}\epsilon(k) \tag{30}$$

$$b_1\omega_{\text{rest}}(k)+b_2\omega_{\text{rest}}(k-1)=a_1\epsilon(k)+a_2\epsilon(k-1) -c_1\epsilon(k)-c_2\epsilon(k-1) \tag{31}$$

B. Proposed Outer Voltage Control Framework

The $d-q$ axis based control architecture of RSC control loops allows the independent control of real and reactive power. For reactive power control, the outer stator terminal voltage control loop derives the reactive power reference. As the machine parameter varies, the estimated rotor speed differs from actual. Since the vector control approach relies on measured values of rotor current and speed, any form of parameter variation can be said to affect the performance capability of conventional vector control approach. Reactive power on stator side is given by

$$Q_s=V_{qs}i_{ds}-V_{ds}i_{qs}. \tag{32}$$

According to the convention, $d-q$ reference frame is assumed to be oriented along stator flux. Thus, the abovementioned reactive power equation can be modified as follows:

$$Q_s=-\frac{V_{qs}\psi_{ds}}{L_s}+\frac{V_{qs}L_m}{L_s}i_{dr}. \tag{33}$$

A portion of this total rotor current is responsible for maintaining terminal voltage through reactive power generation while the other part contributes toward magnetization. The effect of Lm on rotor current and hence the reactive power on stator is shown in (33). The ability of the proposed architecture is that it ensures superior dynamic reactive power support capability even during parameter variations.

C. Proposed Adaptive RSC Control Framework

The dq reference frame based RSC control aims at providing independent control of the active power and reactive power output from stator. The rotor voltage equations that govern the design of RSC control is given by

$$\mathrm{v}'_{\mathrm{drc}} = \mathrm{r}'_{\mathrm{r}}\mathrm{i}'_{\mathrm{dr}} + \mathrm{p}\frac{\sigma \mathrm{L}'_{\mathrm{r}}\mathrm{i}'_{\mathrm{dr}}}{\omega_{\mathrm{b}}} - \omega_{\mathrm{slip}}\left(\frac{\sigma \mathrm{L}_{\mathrm{s}}\mathrm{L}'_{\mathrm{r}}}{\mathrm{L}_{\mathrm{m}}}\mathrm{i}_{\mathrm{qs}} - \frac{\mathrm{r}_{\mathrm{s}}\mathrm{L}'_{\mathrm{r}}}{\mathrm{L}_{\mathrm{m}}}\mathrm{i}_{\mathrm{ds}}\right)$$

$$\mathrm{v}'_{\mathrm{qrc}} = \mathrm{r}'_{\mathrm{r}}\mathrm{i}'_{\mathrm{qr}} + \mathrm{p}\frac{\sigma \mathrm{L}'_{\mathrm{r}}\mathrm{i}'_{\mathrm{qr}}}{\omega_{\mathrm{b}}} - \cdots$$

$$\cdots \omega_{\mathrm{slip}}\left(\frac{\sigma \mathrm{L}_{\mathrm{s}}\mathrm{L}'_{\mathrm{r}}}{\mathrm{L}_{\mathrm{m}}}\mathrm{i}_{\mathrm{ds}} - \frac{\mathrm{L}'_{\mathrm{r}}}{\mathrm{L}_{\mathrm{m}}}\left(\mathrm{v}_{\mathrm{qs}} + \mathrm{r}_{\mathrm{s}}\mathrm{i}_{\mathrm{qs}}\right)\right) \tag{34}$$

where $\sigma = \dfrac{\mathrm{L}'_{\mathrm{r}}\mathrm{L}_{\mathrm{s}} - \mathrm{L}_{\mathrm{m}}^2}{\mathrm{L}_{\mathrm{s}}\mathrm{L}'_{\mathrm{r}}}$. The abovementioned equation can be represented as two components

$$\mathrm{v}'_{\mathrm{drc}} = \mathrm{v}''_{\mathrm{drc}} + \mathrm{v}'''_{\mathrm{drc}} \tag{35}$$

$$\mathrm{v}'_{\mathrm{qrc}} = \mathrm{v}''_{\mathrm{qrc}} + \mathrm{v}'''_{\mathrm{qrc}} \tag{36}$$

and

$$\mathrm{v}''_{\mathrm{drc}} = \left(\mathrm{r}'_{\mathrm{r}} + \mathrm{p}\frac{\sigma \mathrm{L}'_{\mathrm{r}}}{\omega_{\mathrm{b}}}\right)\mathrm{i}'_{\mathrm{dr}}$$

$$\mathrm{v}'''_{\mathrm{drc}} = -\omega_{\mathrm{slip}}\left(\frac{\sigma \mathrm{L}_{\mathrm{s}}\mathrm{L}'_{\mathrm{r}}}{\mathrm{L}_{\mathrm{m}}}\mathrm{i}_{\mathrm{qs}} - \frac{\mathrm{r}_{\mathrm{s}}\mathrm{L}'_{\mathrm{r}}}{\mathrm{L}_{\mathrm{m}}}\mathrm{i}_{\mathrm{ds}}\right)$$

$$\mathrm{v}''_{\mathrm{qrc}} = \left(\mathrm{r}'_{\mathrm{r}} + \mathrm{p}\frac{\sigma \mathrm{L}'_{\mathrm{r}}}{\omega_{\mathrm{b}}}\right)\mathrm{i}'_{\mathrm{qr}}$$

$$\mathrm{v}'''_{\mathrm{qrc}} = -\omega_{\mathrm{slip}}\left(\frac{\sigma \mathrm{L}_{\mathrm{s}}\mathrm{L}'_{\mathrm{r}}}{\mathrm{L}_{\mathrm{m}}}\mathrm{i}_{\mathrm{ds}} + \frac{\mathrm{L}'_{\mathrm{r}}}{\mathrm{L}_{\mathrm{m}}}\left(\mathrm{v}_{\mathrm{qs}} + \mathrm{r}_{\mathrm{s}}\mathrm{i}_{\mathrm{qs}}\right)\right) \tag{37}$$

where v''_{drc} and v''_{qrc} are the control input sequence from conventional RSC control that regulates the output active and reactive power of DFIG.

As the abovementioned sensorless approach is dependent on current sensor measurements [29] and its performance can be impacted due to defective current sensors, the RSC control architecture is modified with an adaptive control framework to improve the robustness of the controller. For this design, the RSC adaptive control loop input sequence $\mathrm{V}''_{\mathrm{dqa}}(\mathrm{k})$ is generated based on (38) with A and B matrix identified between the input $\mathrm{V}''_{\mathrm{dq}}(\mathrm{k})$ and $\epsilon_E(k)$ as the output error using RLS identification detailed in Section III-A2. The output error can be the rotor speed error in active power control and reactive power error in the reactive power control loop. This can be represented as follows:

$$\mathrm{V}''_{\mathrm{dqa}}(\mathrm{k}) = \frac{A(z^{-1})}{B(z^{-1})} \times \epsilon_E(k) \tag{38}$$

where

$$\mathrm{A}(\mathrm{z}^{-1})\epsilon_E(k) = \mathrm{B}(\mathrm{z}^{-1})\mathrm{V}''_{\mathrm{dqa}}(\mathrm{k}) \tag{39}$$

with

$$\mathrm{A}(\mathrm{z}^{-1}) = 1 + \mathrm{a}_1\mathrm{z}^{-1} + \mathrm{a}_2\mathrm{z}^{-2} + \cdots + \mathrm{a}_{\mathrm{n}}\mathrm{z}^{-\mathrm{n}} \tag{40}$$

$$\mathrm{B}(\mathrm{z}^{-1}) = \mathrm{b}_1\mathrm{z}^{-1} + \mathrm{b}_1\mathrm{z}^{-2} + \cdots + \mathrm{b}_{\mathrm{n}}\mathrm{z}^{-\mathrm{n}} \tag{41}$$

and $k = n+1, n+2, \ldots, t$, t being the time index.

The main advantage of the proposed architecture is that it provides a wider operating range and improves the overall stability margin. Also, the approach provides convergence properties in the wake of sensor malfunction or dynamic grid events due to the better estimation of $V''_{dqa}(k)$.

Now the modified RSC control with adaptive input sequence assumes the following form,

$$\mathrm{v}'_{\mathrm{dr}} = \mathrm{v}''_{\mathrm{drc}} + \mathrm{v}''_{\mathrm{dra}} + \mathrm{v}'''_{\mathrm{drc}} \tag{42}$$

$$\mathrm{v}'_{\mathrm{qr}} = \mathrm{v}''_{\mathrm{qrc}} + \mathrm{v}''_{\mathrm{qra}} + \mathrm{v}'''_{\mathrm{qrc}}. \tag{43}$$

The stator real and reactive power output for the modified RSC control is given by

$$\mathrm{P}_{\mathrm{s}} = \frac{\mathrm{L}_{\mathrm{m}}\mathrm{v}_{\mathrm{qs}}}{\mathrm{L}_{\mathrm{s}}}\left(\frac{\mathrm{v}''_{\mathrm{qrc}} + \mathrm{v}''_{\mathrm{qra}}}{\mathrm{r}_{\mathrm{r}} + \mathrm{p}\dfrac{\sigma \mathrm{L}_{\mathrm{r}}}{\omega_{\mathrm{b}}}}\right)$$

$$\mathrm{Q}_{\mathrm{s}} = -\frac{v_{qs}\Psi_{ds}}{L_s} + \frac{\mathrm{L}_{\mathrm{m}}\mathrm{v}_{\mathrm{qs}}}{\mathrm{L}_{\mathrm{s}}}\left(\frac{\mathrm{v}''_{\mathrm{drc}} + \mathrm{v}''_{\mathrm{dra}}}{\mathrm{r}_{\mathrm{r}} + \mathrm{p}\dfrac{\sigma \mathrm{L}_{\mathrm{r}}}{\omega_{\mathrm{b}}}}\right). \tag{44}$$

Equation (44) shows that stator real and reactive power output of a DFIG can be controlled by properly defining the $\mathrm{v}''_{\mathrm{qr}}$ and $\mathrm{v}''_{\mathrm{dr}}$ components of rotor voltages from both conventional vector and adaptive control architectures.

IV. Experimental Results

For the experimental results, we use a GE 1.5 MW wind turbine (WT) model in the real-time simulator (OPAL-RT platform) and a 2 KW WTG (4 quadrant dc motor drive and a wound rotor induction machine- Lab-Volt 8013-A, https://youtu.be/pFkJSz9lFDg) for the hardware-in-the-loop (HIL) test set up that characterizes the GE 1.5 MW model. The specifications are included in Tables III and IV, respectively. The models and the hardware WTG is integrated with the simulator. The RSC and GSC are also integrated into the controller that is designed using the real-time simulator. For sensing, a data acquisition kit (OP 8660) is used. A three-phase power supply integrated with the simulator is used to connect with the grid as a rigid infinite source for the first set of experiments. For the second set of experiments, the rigid source is controlled by an external signal derived from the real-time grid model (IEEE 123 bus system) designed in the real-time simulator. The details are shown in Fig. 4. This is a fully integrated HIL (both power and control) testbed.

The performance of the proposed architecture is validated based on two sets of experiments:

1) The first experimental test set analyzes the performance of the system in a real-time simulation platform with a hard grid (single machine infinite bus mode). We call this a test set 1.
2) The second set is to analyze the performance on a scaled test system with a power grid connected to the WTG. We call this as the test set 2.

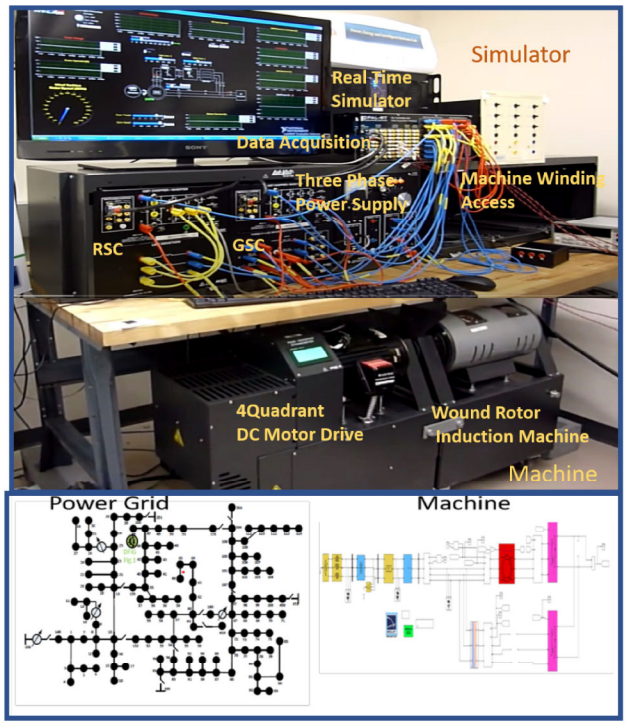

Fig. 4. Schematic of HIL real-time simulations performed with OPAL-RT.

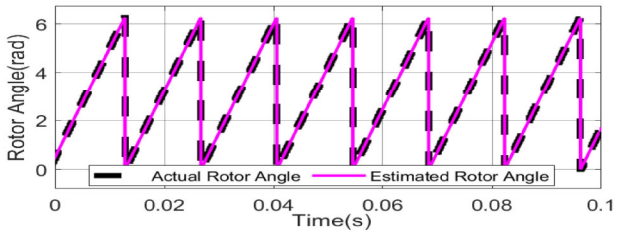

Fig. 5. Case A: Rotor angle (rad) for $1.5L_m$ increase.

A. Test Set 1

In this test set, five cases are performed. Case A evaluates the performance due to machine parameter variation. Case B tests the performance of the proposed controller with a change in terminal voltage. Cases C and D validate the dynamic reactive power support capability during faults and the LVRT, respectively. Case E analyze the robustness of the proposed speed observer to rotor current sensor failure.

1) Case A: Performance Validation With Change in Mutual Inductance: The robustness of the proposed adaptive architecture during parametric changes is evaluated in this case. The performance comparison is with MVC architecture. The test case is performed with a 50% increase and a 30% decrease of machine mutual inductance from its nominal value. The rotor angle estimated with $1.5L_m$ is shown in Fig. 5. Fig. 6 shows that the $\pm 6^\circ$ offset in the MVC architecture is eliminated by the proposed architecture which is one of the major features of the proposed framework. The percentage rotor speed estimation error in Fig. 7 shows the efficiency of the speed estimation by

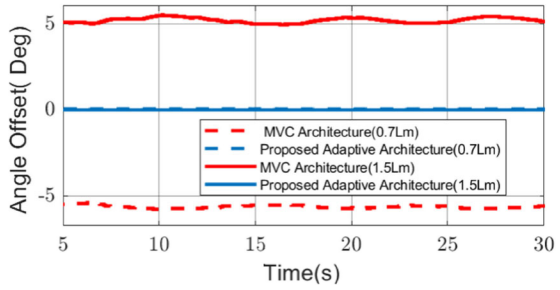

Fig. 6. Case A: Angle offset error(deg) for 1.5 and 0.7 L_m change.

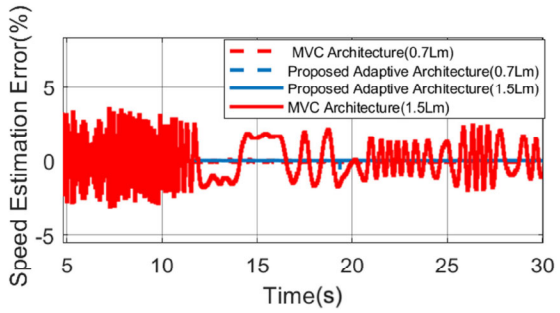

Fig. 7. Case A: Rotor speed estimation error for 1.5 and 0.7 L_m change.

TABLE I
RELATIVE ERROR COMPARISON

	Lm Change	MVC Architecture	Proposed Architecture
Angle Offset Error(deg)	0.7Lm	-6	0.055
Angle Offset Error(deg)	1.5Lm	6	-0.0003
Speed Estimation Error(%)	0.7Lm	± 0.2	± 0.005
Speed Estimation Error(%)	1.5Lm	± 2.5	± 0.0022

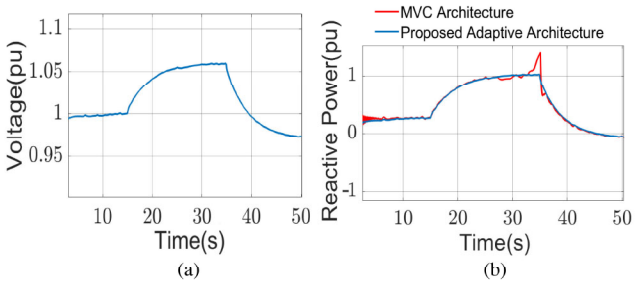

Fig. 8. (a) Case B: Stator terminal voltage. (b) Case B: Comparison of reactive power supplied.

the proposed architecture. A comparative analysis is presented in Table I. The results indicate the ability of the proposed architecture to track the rotor angle effectively.

2) Case B: Performance Validation With Change in Terminal Voltage: The ability of the modified terminal voltage loop is analyzed for a given terminal voltage profile. The terminal voltage variations demanded by a dynamic grid condition are shown in Fig. 8(a). The proposed modified adaptive control architecture can meet the additional reactive power demand to

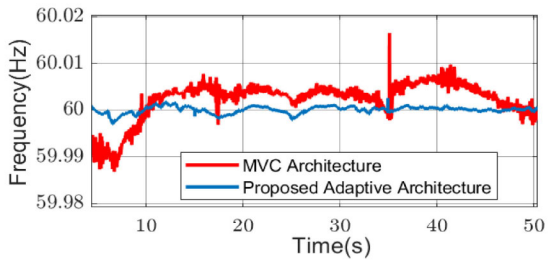

Fig. 9. Case B: Frequency variations of stator terminal voltage.

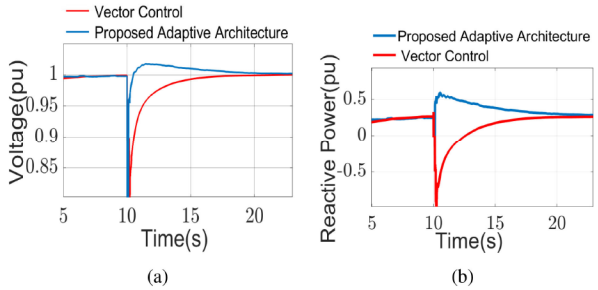

Fig. 10. (a) Case C: Point of common coupling (PCC) voltage during three phase to ground fault. (b) Case C: Reactive power support during fault.

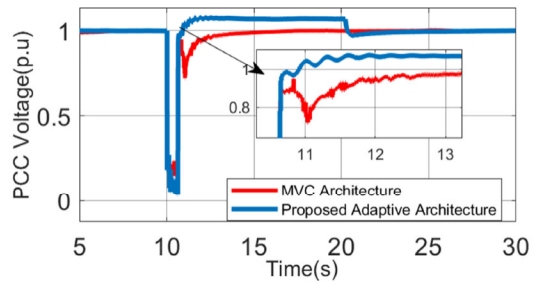

Fig. 11. Case D: PCC voltage during ride through.

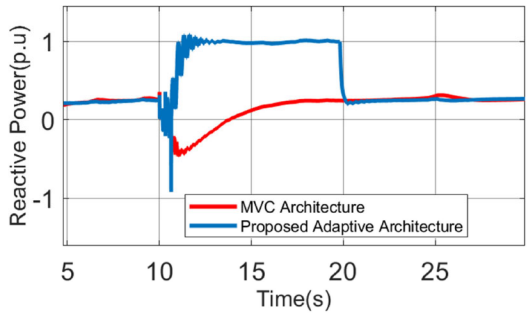

Fig. 12. Case D: Reactive power offered during ride through.

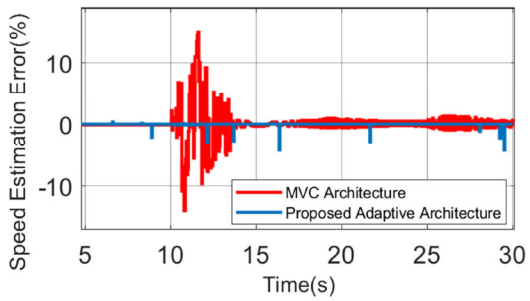

Fig. 13. Case D: Speed estimation error during LVRT with a L_m change.

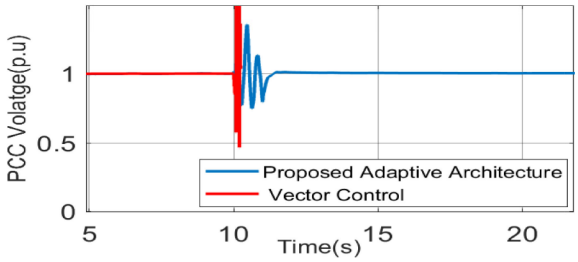

Fig. 14. Case E: Terminal voltage during rotor current sensor failure.

maintain the desired voltage irrespective of the variations in the physical parameters as shown in Fig. 8(b). The superiority of the proposed system to tightly maintain the frequency within $\pm 0.15\%$ is shown in Fig. 9.

3) Case C: Reactive Power Support During Faults: The ability of the modified terminal loop to perform proper reactive power support during grid faults irrespective of any variations in the parameter is analyzed in this case study. The faster response of the proposed system for three-phase fault applied at 10 s when compared with the vector control approach is visible from Fig. 10(a). The reactive power support from the proposed system is showcased in Fig. 10(b). In contrast to the vector control loop, the proposed control loop showcases excellent dynamic stability.

4) Case D: Performance Validation With Low Voltage Ride-Through (LVRT) Capability: The LVRT capability of the proposed architecture is analyzed for $1.5L_m$ in this case study and the comparison is presented with MVC architecture and the conventional voltage control scheme. The stator terminal voltage following a low voltage is showcased in Fig. 11. The modified loop brings the terminal voltage back to the nominal value faster following a disturbance. A small 4% overshoot of terminal voltage is observed from the nominal value which is due to the additional dynamic power support offered by the proposed control loop. The reactive support is within the permissible limit (see Fig. 12). The ability of the proposed architecture to effectively estimate the speed during a grid event is depicted by the speed estimation shown in Fig. 13. The graph has some peaks which are caused due to angle offset estimation error (observed to have a zero impact on DFIG operation as the error is low in magnitude -less than 5% and has a faster ramp- less than milliseconds), yet shows the advantages of proposed control (less than 4%) speed estimation error over conventional MVC based control which has almost 15% error.

5) Case E: Performance Validation During Rotor Current Sensor Failure: Performance efficiency is analyzed using a rotor current sensor failure scenario created at 10 s for a duration of 1 s. With no rotor current measurement data available, the performance of the proposed control architecture is compared to our earlier work [29]. As the proposed control loop can dynamically adjust the variation in feedback current due to current sensor failure, it was observed that the proposed approach can still maintain a stable operation as shown in Fig. 14.

Fig. 15 shows the stability property of the proposed control architecture without any current feedback. It can be seen that the

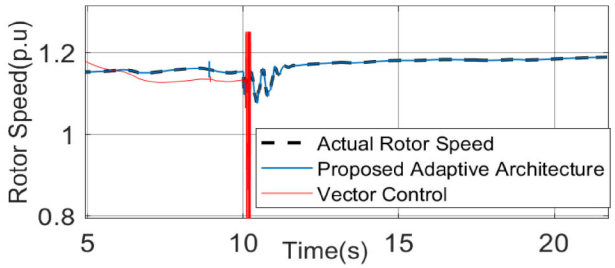

Fig. 15. Case E: Estimated rotor speed during rotor current sensor failure.

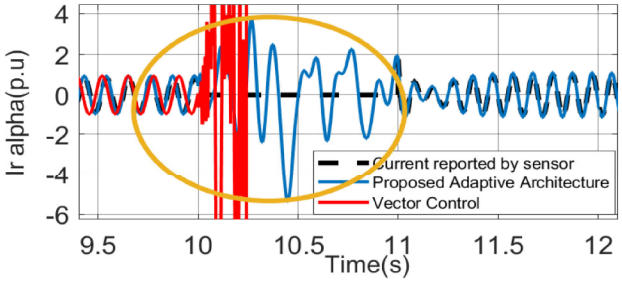

Fig. 16. Case E: Comparison of rotor current in alpha frame during rotor current sensor failure.

TABLE II
SCALABILITY TEST RESULTS

	Value	
Case A	Speed Estimation Error(%)	$\pm 0.005\%$
Case B	Voltage profile Improvement(%)	$\pm 0.66\%$

vector control loses its stability after 10 s which can disconnect DFIG from the grid. Thus, the proposed approach can be economical by avoiding uncontrolled WT downtimes due to sensor failures. Fig. 16 shows the alpha component of the rotor current during the sensor failure. In Fig. 16, when the actual rotor current value is zero due to sensor failure, the proposed control is still able to estimate the rotor current by properly defining the control input sequence to the RSC loop. This assures the robustness of the proposed control to sensor failures. It was also observed that the speed estimation error shows a 50% improvement when compared to vector control.

B. *Test Set 2: Scalability Test*

The performance evaluation of the proposed architecture connected to a real-life grid is validated using a scalability test performed on the 123bus system with HIL. Fig. 17 shows the one-line diagram of the test system used to perform the test cases. Case A analyses the performance of the controller during parameter variation. Case B analyses the performance during a sudden load change. Table II summarizes the results of the scalability test. The reason for testing with the real-grid is to evaluate the performance when the dynamics are realistic as opposed to a rigid voltage source.

1) Case A: Performance Validation With Parameter Variation: This case validates the ability of the controller to nullify the effects of parameter variations in a real grid environment. All the test results are presented for the proposed system with a 50% increase and a 30% decrease in mutual inductance. Fig. 18(a) shows the ability of the controller to efficiently estimate the speed with an error as low as $\pm 0.005\%$. Fig. 18(b) shows that the proposed system can effectively estimate the rotor speed even in a scaled system without being impacted by side effects of parameter variations.

2) Case B: Performance Validation With Sudden Load Change: Case B analyses the performance of the system during

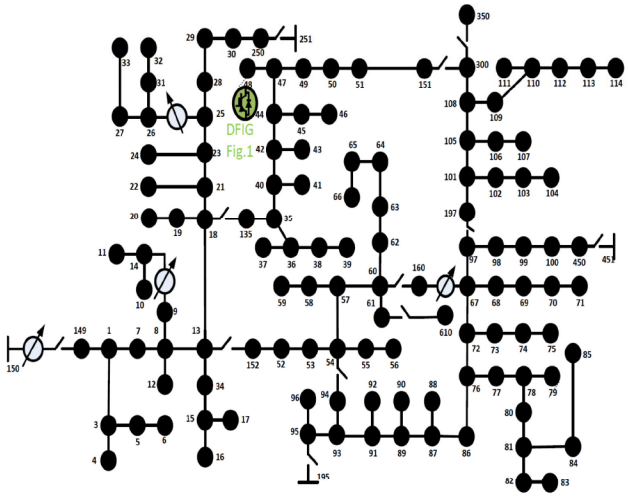

Fig. 17. One line diagram of the test system used to perform scalability test.

TABLE III
DFIG PARAMETERS

Parameter	Value
Rated Capacity	1.5 MVA
Rated Voltage	575 V L-L
Stator resistance (r_s)	0.0071 p.u.
Stator ref. rotor resistance (r'_r)	0.005 p.u.
Stator leakage inductance (L_{ls})	0.1714 p.u.
Stator ref. rotor leakage inductance (L'_{lr})	0.1563 p.u.
Mutual inductance (L_m)	5.8 p.u.
Number of pole pairs (p)	3
Inertia Constant (H)	0.5 s
Simulation Time Step (T_s)	50 μs
Identification Time Step (T_i)	5 ms
MVC Time Step (T_c)	2 ms
Grid coupling inductor	1mH
Grid frequency	60Hz

TABLE IV
PARAMETERS OF WOUND ROTOR INDUCTION MACHINE (WRIM) USED IN HIL

Parameter	Value
Rated Capacity	2 KW
Rated Voltage	120/208 V
Rotor Winding Voltage	624 V L-L
Stator resistance (r_s)	0.6 Ω
Rotor resistance (r_r)	4.3 Ω
Power factor	0.72
Number of pole pairs (p)	2
Simulation Time Step (T_s)	50 μs
Rated frequency	60Hz

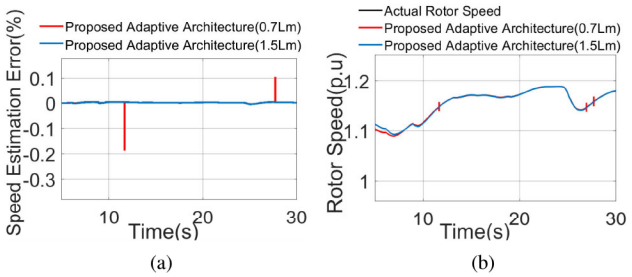

Fig. 18. (a) Case A: Speed estimation error during an L_m change. (b) Case A: Estimated rotor speed during an L_m change.

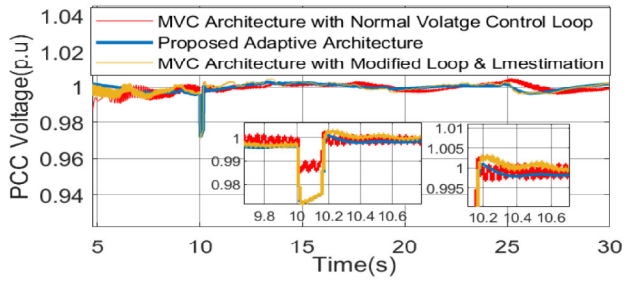

Fig. 19. Case B: PCC voltage during sudden load change.

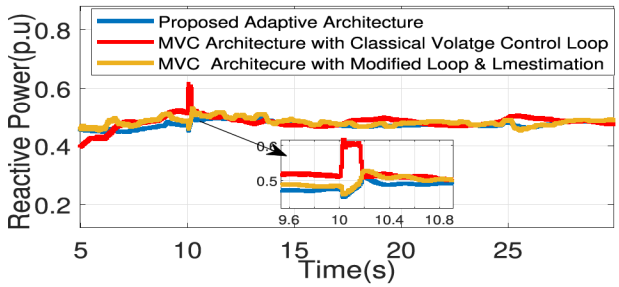

Fig. 20. Case B: Reactive power during sudden load change.

a sudden load change initiated at 10 s for a very short duration with a 50% increase in machine mutual inductance. The test results compare the performance of proposed architecture first with MVC based on normal voltage control loop and no Lm estimation, and, second with MVC based on modified voltage loop and Lm estimation. Figs. 19 and 20 show the PCC voltage and reactive power support offered by the system during the event. It can be noted that the proposed system can maintain the terminal voltage faster to the desired nominal value with minimal reactive power support. Also, larger oscillations are observed on MVC control without a Lm estimation. This clearly shows the importance of parameter estimation to improve power quality. The reactive power output in Fig. 20 shows that MVC with no Lm estimation demands more reactive power to maintain the PCC voltage to the desired value. Fig. 21(a) compares mutual inductance. It can be seen that the estimated inductance is close to machines inductance during a Lm increase with $\pm 2\%$ precision. Fig. 21(b) compares the angle estimation error for all three controllers. It can be seen that the proposed controllers

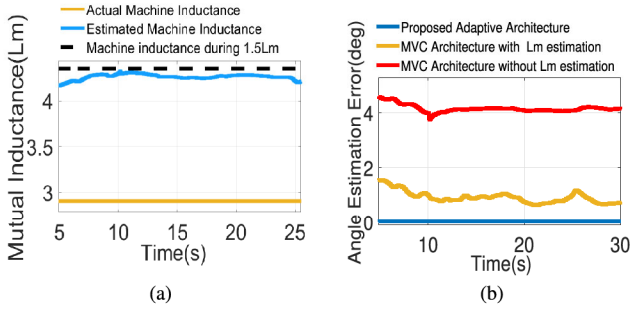

Fig. 21. (a) Case B: Estimated mutual inductance used by outer voltage loop during sudden load change. (b) Case B: Comparison of rotor angle estimation error for proposed adaptive architecture with and without Lm estimation based MVC architecture.

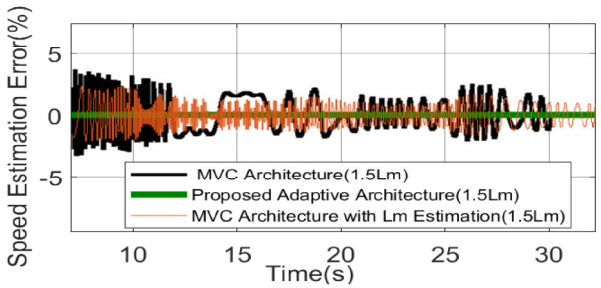

Fig. 22. Comparison of speed estimation error for proposed adaptive architecture with Lm estimation based MVC architecture.

show very close to zero angle error depicting the accuracy of estimating the rotor angle and speed during parameter variations.

V. Conclusion

This article proposes a novel adaptive control and speed estimation technique. The proposed estimation based speed observer technique can overcome the angle offset error due to parameter variation of DFIG. The modified reactive power reference generation loop ensures accurate reactive power reference irrespective of the variations in mutual inductance. The modified adaptive RSC loop ensures the robustness of the proposed architecture to current sensor failure apart from mechanical sensors mentioned in earlier work. Moreover, the proposed system does not demand any additional control loop to estimate parameters which considerably increases the accuracy of estimation. Fig. 22 shows the proposed methods have speed estimation error as low as 0.001% while the normal MVC with Lm estimation shows up to 2% error. The use of an identification based self-tuning controller ensures a wider operating range, faster performance, and improved reliability in comparison to static controllers. The experimental validations based on real-time simulations as well as the scalability test validates the superior performance features of the proposed modified controller and estimation technique.

References

[1] R. Datta and V. T. Ranganathan, "A simple position-sensorless algorithm for rotor-side field-oriented control of wound-rotor induction machine," *IEEE Trans. Ind. Electron.*, vol. 48, no. 4, pp. 786–793, Aug. 2001.

[2] L. Morel, H. Godfroid, A. Mirzaian, and J. M. Kauffmann, "Double-fed induction machine: Converter optimisation and field oriented control without position sensor," *IEE Proc. Electric Power Appl.*, vol. 145, no. 4, pp. 360–368, 1998.
[3] R. Cardenas, R. Pena, J. Proboste, G. Asher, and J. Clare, "MRAS observer for sensorless control of standalone doubly fed induction generators," *IEEE Trans. Energy Convers.*, vol. 20, no. 4, pp. 710–718, Dec. 2005.
[4] M. Pattnaik and D. Kastha, "Adaptive speed observer for a stand-alone doubly fed induction generator feeding nonlinear and unbalanced loads," *IEEE Trans. Energy Convers.*, vol. 27, no. 4, pp. 1018–1026, Dec. 2012.
[5] A. Susperregui, M. I. Martinez, G. Tapia, and I. Vechiu, "Second-order sliding-mode controller design and tuning for grid synchronisation and power control of a wind turbine-driven doubly fed induction generator," *IET Renewable Power Gener.*, vol. 7, no. 5, pp. 540–551, 2013.
[6] G. D. Marques, D. M. Sousa, and M. F. Iacchetti, "Air-gap power-based sensorless control in a DFIG connected to a dc link," *IEEE Trans. Energy Convers.*, vol. 30, no. 1, pp. 367–375, Mar. 2015.
[7] Longya Xu and Wei Cheng, "Torque and reactive power control of a doubly fed induction machine by position sensorless scheme," *IEEE Trans. Industry Appl.*, vol. 31, no. 3, pp. 636–642, May/Jun. 1995.
[8] D. D. Reigosa, F. Briz, C. Blanco, and J. M. Guerrero, "Sensorless control of doubly fed induction generators based on stator high-frequency signal injection," *IEEE Trans. Industry Appl.*, vol. 50, no. 5, pp. 3382–3391, Jan. 2014.
[9] D. D. Reigosa, F. Briz, C. Blanco Charro, A. Di Gioia, P. Garca, and J. M. Guerrero, "Sensorless control of doubly fed induction generators based on rotor high-frequency signal injection," *IEEE Trans. Industry Appl.*, vol. 49, no. 6, pp. 2593–2601, May 2013.
[10] M. Szypulski and G. Iwanski, "Sensorless state control of stand-alone doubly fed induction generator supplying nonlinear and unbalanced loads," *IEEE Trans. Energy Convers.*, vol. 31, no. 4, pp. 1530–1538, Dec. 2016.
[11] K. Luo, W. Shi, and J. Qu, "Multi-machine equivalent model parameter identification method for double-fed induction generator (DFIG)-based wind power plant based on measurement data," *J. Eng.*, vol. 2017, no. 13, pp. 1550–1554, 2017.
[12] E. Torres, S. Djurovic, V. Terzija, and S. Williamson, "Application of parameter estimation methods to the assessment of DFIG;s currents," in *Proc. IEEE Bucharest PowerTech*, 2009, pp. 1–6.
[13] A. Parida and D. Chatterjee, "A robust parameter non-sensitive rotor position and speed estimator for DFIG," in *Proc. Int. Conf. Control, Instrum., Energy Commun.*, 2014, pp. 12–16.
[14] A. Djoudi, H. Chekireb, and S. Bacha, "On-line identification of DFIG parameters with rotor current reconstitution," in *Proc. 9th Int. Conf. Ecological Vehicles Renewable Energies.*, 2014, pp. 1–6.
[15] D. Li, X. Lin, S. Hu, and Y. Kang, "An adaptive estimation method for parameters of doubly-fed induction generators (DFIG) in wind power controller," in *Proc. Asia-Pacific Power Energy Eng. Conf.*, 2010, pp. 1–4.
[16] A. Djoudi, H. Chekireb, E. Berkouk, and S. Bacha, "Real time estimation of DFIG inductances and rotor currents," in *Proc. 3rd Renewable Power Gener. Conf.*, 2014, pp. 1–5.
[17] L. Lu, N. F. Avila, C. Chu, and T. Yeh, "Model reference adaptive back-electromotive-force estimators for sensorless control of grid-connected DFIGs," *IEEE Trans. Industry Appl.*, vol. 54, no. 2, pp. 1701–1711, Mar./Apr. 2018.
[18] X. Wang, Jian Xiong, L. Geng, J. Zheng, and S. Zhu, "Parameter identification of doubly-fed induction generator by the levenberg-marquardt-fletcher method," in *Proc. IEEE Power Energy Soc. Gen. Meeting*, 2013, pp. 1–5.
[19] H. Junxian *et al.*, "The dynamic simulation model and parameter identification method of DFIG type wind generator for power system electro-mechanic simulation," in *Proc. IEEE PES Asia-Pacific Power Energy Eng. Conf.*, 2014, pp. 1–6.
[20] R. Maharjan and S. Kamalasadan, "A novel online adaptive sensorless identification and control of doubly fed induction generator," in *Proc. IEEE PES Gen. Meeting|Conf. Expo.*, Jul. 2014, pp. 1–5.
[21] R. Bhattarai, N. Gurung, and S. Kamalasadan, "Minimum variance controller based adaptive control for doubly fed induction generator," in *Proc. North Amer. Power Symp.*, Sep. 2016, pp. 1–6.
[22] R. Bhattarai, N. Gurung, S. Ghosh, and S. Kamalasadan, "Parametrically robust dynamic speed estimation based control for doubly fed induction generator," *IEEE Trans. Industry Appl.*, vol. 54, no. 6, pp. 6529–6542, Nov. 2018.
[23] R. Bhattarai, N. Gurung, S. Ghosh, and S. Kamalasadan, "Parametrically robust dynamic speed estimation based control for doubly fed induction generator," in *Proc. IEEE Industry Appl. Soc. Annu. Meeting*, 2017, pp. 1–8.
[24] S. Ghosh and S. Kamalasadan, "An integrated dynamic modeling and adaptive controller approach for flywheel augmented DFIG based wind system," *IEEE Trans. Power Syst.*, vol. 32, no. 3, pp. 2161–2171, May 2017.
[25] B. Singh, S. Puchalapalli, S. K. Tiwari, and P. K. Goel, "Variable step HCS based sensorless control of wind driven DFIG for autonomous operation," in *Proc. 2nd IEEE Int. Conf. Power Electron., Intell. Control Energy Syst.*, 2018, pp. 504–509.
[26] M. A. Mossa, A. Saad Al-Sumaiti, T. Duc Do, and A. A. Zaki Diab, "Cost-effective predictive flux control for a sensorless doubly fed induction generator," *IEEE Access*, vol. 7, pp. 172 606–172 627, 2019.
[27] R. M. Prasad and M. A. Mulla, "A novel position-sensorless algorithm for field-oriented control of DFIG with reduced current sensors," *IEEE Trans. Sustain. Energy*, vol. 10, no. 3, pp. 1098–1108, Jul. 2019.
[28] A. T. Nguyen and D. Lee, "Sensorless control scheme of DFIG wind energy conversion systems based on sogis and fll," in *Proc. IEEE 10th Int. Symp. Power Electron. Distrib. Gener. Syst.,*2019, pp. 466–472.
[29] A. R. Nair, R. Bhattarai, and S. Kamalasadan, "Parametrically robust mutual inductance estimation based adaptive control architecture for doubly fed induction generator (DFIG)," in *Proc. IEEE Energy Convers. Congr. Expo.*, 2019, pp. 434–441.
[30] K. Åström and B. Wittenmark, *Adaptive Control* (Series Addison-Wesley Series in Electrical Engineering: Control Engineering). Reading, MA, USA: Addison-Wesley, 1995. [Online]. Available: https://books.google.com/books?id=FJ4eAQAAIAAJ

Anuprabha Ravindran Nair (Graduate Student Member, IEEE) received the B.Tech degree in electrical engineering from Calicut University, Malappuram, India, in 2010, and the M.S. degree in electrical engineering from Purdue University, West Lafayette, IN, USA, in 2016. She has been currently working toward the Ph.D. degree in electrical engineering from the Department of Electrical and Computer Engineering, University of North Carolina at Charlotte, Charlotte, NC, USA, since 2017.

Her research interests include renewable energy integration and stability, doubly fed induction generator based wind energy conversion system, modeling and analysis of weak grid, power system stability and control, integration of distributed energy resources and contribution to power system stability.

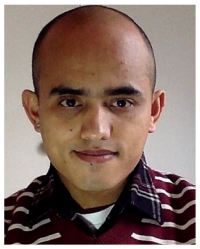

Rojan Bhattarai (Member, IEEE) received the B.E. degree in electrical engineering from the Institute of Engineering, Pulchowk Campus, Tribhuvan University, Kirtipur, Nepal, in 2012 and the Ph.D. degree in electrical engineering from the University of North Carolina at Charlotte, Charlotte, NC, USA, in 2018.

Since then, he has been working as a Postdoctoral Intern with Argonne National Laboratory, Lemont, IL, USA. His current research interests include distributed energy systems modeling, and control and stability studies of renewable integrated power grid.

Sukumar Kamalasadan (Senior Member, IEEE) received the B Tech. degree in electrical and electronics engineering from the University of Calicut, Kerala, India, in 1991, the M. Eng. degree in electrical power systems management from the Asian Institute of Technology, Bangkok, Thailand, in 1999, and the Ph.D. degree in electrical engineering from the University of Toledo, Toledo, OH, USA, in 2004.

He is currently working as a Professor with the Department of Electrical and Computer Engineering, University of North Carolina at Charlotte, Charlotte, NC, USA. His research interests include intelligent and autonomous control, power systems dynamics, stability and control, smart grid, micro-grid and real-time optimization and control of power system

Dr. Kamalasadan has won several awards including the NSF CAREER Award and the IEEE Best Paper Award.